Stress-modulated relaxor-to-ferroelectric transition in lead-free $(Na_{1/2}Bi_{1/2})TiO_3$-$BaTiO_3$ ferroelectrics

Florian H. Schader,[1] Zhiyang Wang,[2,3] Manuel Hinterstein,[2,4] John E. Daniels,[2] and Kyle G. Webber[5]
[1]*Institute of Materials Science, Technische Universität Darmstadt, 64287 Darmstadt, Germany*
[2]*School of Materials Science and Engineering, UNSW Australia, Sydney 2052, Australia*
[3]*Australian Synchrotron, 800 Blackburn Road, Clayton, Victoria 3168, Australia*
[4]*Institute for Applied Materials, Karlsruhe Institute for Technology, P.O. Box 3640, 76021 Karlsruhe, Germany*
[5]*Department of Materials Science, Friedrich-Alexander-Universität Erlangen-Nürnberg, 91058 Erlangen, Germany*
(Received 5 January 2016; revised manuscript received 17 March 2016; published 20 April 2016)

The effect of external mechanical fields on relaxor $0.94(Na_{1/2}Bi_{1/2})TiO_3$-$0.06BaTiO_3$ was investigated by means of temperature- and stress-dependent dielectric constant measurements between 223 and 673 K. Analogous to previous investigations that showed an electric-field-induced ferroelectric long-range order in relaxor ferroelectrics, we show that compressive stress can also result in the transition to the long-range ferroelectric order, marked by the formation of an anomaly in the permittivity-temperature curves and a nonlinear, remanent change in permittivity during mechanical loading. *In situ* stress-dependent high-energy x-ray diffraction experiments were performed at room temperature and reveal an apparent phase transition during mechanical loading, consistent with previous macroscopic electrical measurements. The transition lines between the relaxor states and the stress-induced ferroelectric state were determined at constant temperatures with stress-dependent dielectric constant measurements, providing a stress-temperature phase diagram.

DOI: 10.1103/PhysRevB.93.134111

I. INTRODUCTION

$(Na_{1/2}Bi_{1/2})TiO_3$-based (NBT) lead-free ferroelectric materials have been shown to display exceptionally large unipolar strain response, which is potentially useful in off-resonance actuation applications [1–4]. Solid solutions of NBT, ferroelectric rhombohedral ($R3c$) [5], and $BaTiO_3$ (BT), ferroelectric tetragonal ($P4mm$), form a morphotropic phase boundary (MPB) at BT concentrations of 6−7 mol % at room temperature [6–8]. At room temperature NBT-xBT compositions at the MPB display typical ferroelectric polarization– and strain–electric-field hysteresis loops expected for conventional ferroelectrics [9–11]. With an increase in temperature, however, there is a loss in remanent strain and a retention of the large maximum strain, resulting in a large yet temperature-dependent unipolar strain response [9,12,13].

There has been considerable work on the origins of this large electromechanical coupling, which has been proposed to be an electric-field-induced transition from the initial relaxor state to a state with long-range ferroelectric order [8,14]. *In situ* diffraction studies have revealed that NBT-0.06BT lacks a typical ferroelectric domain structure in the virgin state [15,16] and possesses a pseudocubic phase structure [17,18]. With the application of an electric field, however, an apparent phase transition to a lower-symmetry phase and the formation of metastable ferroelectric domains was found [6,8,16,18,19], corresponding to a large increase in polarization and strain. At temperatures below the freezing temperature (T_f), NBT-0.06BT is considered to be a nonergodic relaxor that undergoes a metastable relaxor-ferroelectric (RE-FE) transition under an electric field. The transition temperature $T_{F\text{-}R}$ is often defined as the temperature during heating when the thermal fluctuations are large enough to break the electric-field-induced order, resulting in a significant decrease in the small signal piezoelectric response of a poled ferroelectric material [20]. However, it was found in previous investigations [21–24] that T_f and $T_{F\text{-}R}$ do not necessarily need to coincide, i.e., the macroscopically poled domain structure thermally depoles at T_f but only at the (higher) $T_{F\text{-}R}$ disintegrates into polar nanoregions (PNRs). With an increasing temperature above the depolarization temperature, NBT-0.06BT is in an ergodic relaxor state. Interestingly, although the transition from the nonergodic to the ergodic state cannot be measured with temperature-dependent x-ray diffraction (XRD), as the material appears pseudocubic in the unpoled state, impulse resonance spectroscopy clearly shows an elastic modulus softening in the vicinity of the depolarization temperature, which typically indicates a structural phase transition [25,26]. In the ergodic relaxor state, the long-range order induced by the electric field is unstable and a converse transition to the relaxor state during unloading is observed. This reversible transition from the macroscopically nonpolar state to the macroscopically polar state is the origin of the large unipolar strain [27]. Similar observations of dielectric anomalies at the depolarization temperature and ability to induce metastable long-range ferroelectric order with an external electric field have been made on lead-containing relaxors, such as $Pb_{1-x}La_x(Zr_yTi_{1-y})_{1-x/4}O_3$, $Pb(Mg_{1/3}Nb_{2/3})O_3$, and $(1-x)Pb(Mg_{1/3}Nb_{2/3})O_3$-$xPbTiO_3$ [28–31].

There remains considerable debate about the structural origins of relaxor properties, in particular the existence and influence of PNRs [32]. Optical microscopy and x-ray diffraction studies have not been able to clearly show a macroscopic phase transition as is observed in conventional ferroelectrics. Diffraction and optic index of refraction studies, however, have observed correlated clusters appearing below approximately 600 K in polycrystalline $Pb(Mg_{1/3}Nb_{2/3})O_3$ [33,34] and $(Pb_{1-3x/2}La_x)(Zr_yTi_{1-y})O_3$ [35]. Additionally, high-resolution optical microscopy investigations of $Pb(Mg_{1/3}Nb_{2/3})O_3$ have indicated the existence of ordered nonstoichiometric regions, consisting of Mg^{2+} and Nb^{5+} cations on the B site, which are surrounded by a Nb-rich matrix [36]. Following

investigations, however, revealed that thermal annealing can lead to domain coarsening, which cannot be explained by the space-charge model [37]. Despite the formation of larger domains, the relaxor properties remain, suggesting a charge balanced random-site model.

Although numerous theories have been proposed to explain relaxor behavior, such as the superparaelectric model [38], dipolar glass model [39], random-field theory [40,41], breathing model [42], and random-bond–random-field model [43], it is generally accepted that the relaxor state is induced by local fields, resulting from the cation chemical substitution and lattice defects. At high temperatures, thermal fluctuations are large, preventing the presence of any polar order. At temperatures below the Burns temperature, it is proposed that PNRs develop, which are highly dynamic and not correlated. In this temperature range, the relaxor is referred to as an ergodic relaxor, where the spatially and temporally averaged behavior is the same. With a further decrease in temperature below the freezing temperature (Vogel-Fulcher temperature), the PNR dynamics slow down and the spatially and temporally averaged behavior is no longer the same. This state is referred to as nonergodic relaxor [44]. Due to the slower dynamics, it is possible through the application of a sufficiently large electric field to align the PNRs and subsequently increase their correlation length. This essentially reduces the effect of random fields and results in the formation of macroscopic domains. This phase transition is, however, not metastable in the ergodic state as the thermal fluctuations are too large and any electrically induced polar order is disrupted upon unloading, resulting in the formation of pinched polarization–electric-field hysteresis curves [31].

Utilizing dielectric constant measurements as a function of temperature for samples with a different electrical history, the three primary states, i.e., nonergodic, ergodic, and ferroelectric, can be determined, providing an electric-field–temperature (E-T) phase diagram of a relaxor ferroelectric. E-T phase diagrams have been previously presented for $Pb_{1-x}La_x(Zr_yTi_{1-y})_{1-x/4}O_3$ [28], $Pb(Mg_{1/3}Nb_{2/3})O_3$ [45,46], $(1-x)Pb(Mg_{1/3}Nb_{2/3})O_3$ [47], $(1-x)Pb(Zn_{1/3}Nb_{2/3})O_3$-$x$PbTiO$_3$ [47], and Mn-doped NBT-xBT [48], giving considerable insight into the role of external electric fields on the stability of the relaxor states. Besides the effect of an electric field, Samara reported the influence of hydrostatic mechanical pressure on the phase transition behavior of a relaxor material [49]. It was found that a sufficiently large pressure could inhibit the relaxor-ferroelectric phase transition of $KTa_{1-x}Nb_xO_3$ and $(1-x)Pb(Zn_{1/3}Nb_{2/3})O_3$-$x$PbTiO$_3$ during field cooling. This was rationalized by the pressure dependence for the soft mode frequency of these materials, i.e., the correlation length of the PNRs decreased with increasing hydrostatic stress, preventing the PNRs from percolating and therefore from transforming to a macrodomain, ferroelectric state. There has, however, been little work on the effect of an external uniaxial mechanical field on the relaxor-ferroelectric phase transition. In this study, we clearly show that an external uniaxial compressive stress can induce long-range ferroelectric order in polycrystalline relaxor NBT-0.06BT. Macroscopic data are contrasted with *in situ* stress-dependent high-energy x-ray diffraction results obtained through a comprehensive structure and texture analysis [50] that show an apparent stress-induced phase change, analogous to previous electrical measurements on a similar composition [19]. A stress-temperature phase diagram is proposed, which shows analog characteristics to the electrical case.

II. EXPERIMENTAL METHODOLOGY

Polycrystalline NBT-0.06BT samples were prepared using the conventional mixed oxide route with high-purity starting powders (Alfa Aesar, Heysham, Lancashire, UK) of Bi_2O_3 (99.975%), $NaCO_3$ (99.5%), $BaCO_3$ (99.8%), and TiO_2 (99.6%). The raw powders were filled together with zirconia milling balls and ethanol into polyamide 6.6 milling containers, which were capable holding a batch of 30 g each. The powders were then mixed and ground by a planetary mill (pulverisette 5, Fritsch GmbH, Idar-Oberstein, Germany) for 24 h at 250 rpm. After drying and pestling, the powders were filled into alumina crucibles for a two-step calcination process. The powders were first heated up to 973 K with a rate of 5 K/min and this temperature was then held for 2 h. In the next step, the temperature was increased to 1073 K with a heating rate of 5 K/min and a dwell time of 3 h, followed by furnace cooling. Subsequently, the powders were milled again for 24 h at 250 rpm in ethanol and finally sieved through a 160-μm sieve after complete drying.

Following calcination, NBT-0.06BT powder was uniaxially pressed into green bodies, which were then cold isostatically pressed in oil at 357 MPa for 1.5 min (press: KIP 100 E; oil: HLPD 10, P/O/Weber GmbH, Remshalden, Germany). A latex sealing prevented the green bodies from being contaminated by the pressing fluid. The samples were then sintered in air at 1423 K (heating rate: 5 K/min) for 3 h, followed by furnace cooling. By using a lathe and a surface grinder, the cylindrical samples with a height of 6 mm and diameter of 5.8 mm were ground from the sintered body. Following the shaping procedure, all samples were annealed at 673 K for 30 min to alleviate residual stresses possibly induced by the machining processes. Platinum electrodes were deposited with a sputter coater (Emitech K950X, Quorum Technologies Ltd., Laughton, East Sussex, UK) onto the parallel circular surfaces of the sample. For stress-dependent XRD measurements, polycrystalline cylindrical samples with a height of 2 mm and diameter of 1 mm were prepared with the same processing procedure.

In this work, the temperature- and stress-dependent relative dielectric permittivity and loss tangent as well as direct piezoelectric coefficient were characterized for polycrystalline NBT-0.06BT samples. Prior to zero-field heating measurements, samples were electrically poled or mechanically textured at elevated temperature and field cooled. In this work, the term "field" refers to either mechanical bias stress or electric field. Stress-dependent measurements of the dielectric permittivity were performed on unpoled virgin samples. Additional *in situ* stress-dependent XRD measurements were done on virgin samples at room temperature. The electrically poled samples were poled with 2 kV/mm for 5 min at 423 K in an oil bath and subsequently field cooled to room temperature. For mechanical texturing, the samples were mounted in a screw-driven uniaxial load frame (5967, Instron GmbH, Darmstadt, Germany) and heated to 423 K with an integrated temperature

chamber (TK 26.600.LN2, Fresenberger GmbH, Wipperfürth, Germany), while a compressive preload of −5 MPa was applied to maintain electrical contact. After waiting for the temperature to stabilize at 423 K, the mechanical compressive stress was increased to values between −100 and −500 MPa and held for 5 min or 1 h, followed by cooling down the sample to room temperature with a rate of 3 K/min with the stress still applied. The active cooling was done by a controlled intake of liquid nitrogen into the circulation air of the temperature chamber. For both electrical poling and mechanical texturing, a minimum waiting time of 24 h was used before further measurements.

The temperature-dependent dielectric permittivity and loss of electrically and mechanically poled NBT-0.06BT samples at frequencies between 1 kHz and 1 MHz were characterized with an LCR meter (HP 4284A, Agilent Technologies Inc., Santa Clara, CA). The sample was heated up to 673 K with a rate of 2 K/min in the above-described load frame at a constant preload of −5 MPa, which was required to ensure sample contact. The characterization of the stress-dependent relative permittivity and dielectric loss of unpoled NBT-0.06BT samples at 1 kHz and at constant temperature were performed with the same setup by increasing and decreasing the uniaxial compressive stress up to −600 MPa at a rate of 0.5 MPa/s. All measurement data were recorded by a custom-built LabVIEW program.

Temperature-dependent measurements of the piezoelectric coefficient d_{33} and the dielectric permittivity ε' of poled NBT-0.06BT samples were performed in a uniaxial screw-driven load frame (Z030, Zwick GmbH & Co. KG, Ulm, Germany) with an integrated piezoelectric stack actuator (P-025.80, PI Ceramic GmbH, Lederhose, Germany). The actuator unloaded the sample sinusoidally with an amplitude of ±0.5 MPa at frequencies between 0.1 and 240 Hz at a preload of −5 MPa. The resulting polarization change was measured with a modified Sawyer-Tower circuit. From the load and polarization amplitudes, the small signal direct piezoelectric coefficient could be calculated. Simultaneously to these measurements, the dielectric permittivity was recorded by using an LCR meter (HP 4284A, Agilent). A more detailed description of the experimental setup can be found elsewhere [51].

The high-energy x-ray diffraction experiments were carried out at beamline ID15 of the European Synchrotron Radiation Facility using a monochromatic beam of energy 72.72 keV (wavelength 0.17049 Å). Unpoled NBT-0.06BT samples were loaded in a custom-built load frame capable of applying compressive stresses up to 10 kN. Importantly, the sample aspect ratio (height:diameter) was 2:1, helping to minimize the effects of clamping stresses at the loading surfaces. The sample height and diameter were 2 mm and 1 mm, respectively. A piezoelectric actuator (P-235.80, PI Ceramic GmbH, Lederhose, Germany) mounted in a stiff metal frame applied uniaxial compressive stress to the sample with polished tungsten carbide pressing dies. The contact surface of the dies was flat, while the other side was hemispherical, thereby helping to reduce effects of slight misalignment. The piezoelectric actuator was applied with an electric field by a high-power voltage amplifier (E-481.00, PI Ceramic GmbH). A function generator was used to create a triangular voltage input signal for the amplifier with a maximum voltage of 5 V and frequency of 625 μHz. This loading scheme resulted in a maximum stress on the sample of −593 MPa. The beam size, which was set to approximately 200 × 200 μm^2, passed through the center of the sample. Diffraction images were collected in transmission geometry using a Pixium 4700 flat panel area detector [52] at a rate of 2 Hz during the application of the triangular loading profile. The acquired diffraction images were radially integrated into 36 azimuthal segments of 10° width using the software package fit2D [53]. Under the present scattering geometry, the obtained data represent the diffraction information with the scattering vectors aligned from parallel to perpendicular to the loading direction. Data analysis was performed using the Rietveld refinement program MAUD (materials analysis using diffraction) [54] to describe the structure changes as a function of compressive stress over the entire mechanical loading/unloading cycle. The structural models used in the refinements include a cubic $Pm\bar{3}m$ phase, a tetragonal $P4mm$ phase, and a rhombohedral $R3c$ phase. The texture was refined with an exponential spherical harmonics model and the lattice strain was refined with the WSODF (weighted strain orientation distribution function) model [55]. Detailed information about the refinement procedure of textured piezoceramics can be found elsewhere [50].

III. RESULTS AND DISCUSSION

A. Dielectric response as a function of temperature with varying dc bias stress

Figure 1 shows the relative permittivity of polycrystalline NBT-0.06BT characterized at various frequencies from room temperature up to 673 K on samples with different poling histories. For comparison, the data for the unpoled sample are also shown in Figs. 1(b) and 1(c) as a dotted line for each frequency. During testing each sample was measured during zero-field heating. The dielectric response of the virgin sample shows a frequency response characteristic of NBT-based ferroelectrics [18,29,56], without a dielectric anomaly in the vicinity of the depolarization temperature. As previously shown after electrical poling a clear dielectric anomaly is developed during heating [15,18,29,56], often referred to as the ferroelectric-relaxor transition temperature ($T_{F\text{-}R}$). Similar poling effects have been observed in other relaxor ferroelectrics [28,30,57]. This anomaly is attributed to the formation of a long-range ferroelectric order upon poling. At $T_{F\text{-}R}$ the induced order is destroyed by thermal fluctuations and the material changes to the ergodic relaxor state. This temperature has also been shown to closely correlate to the depolarization temperature, as the ordered domain structure is lost [58]. In the current study, the $T_{F\text{-}R}$ was found to be 350 K, which corresponds well to previously reported values [23]. The poling technique is, however, known to influence the observed transition temperature; in the current study the samples were electrically poled at 423 K, whereas in Ref. [23] the samples were poled at room temperature. The poling process, e.g., poling field, ambient temperature, field cooling, etc., are known to affect the observed $T_{F\text{-}R}$ values [31,57]. With increasing temperature above $T_{F\text{-}R}$ there is the development of frequency dependence, consistent with the suggested relaxor state.

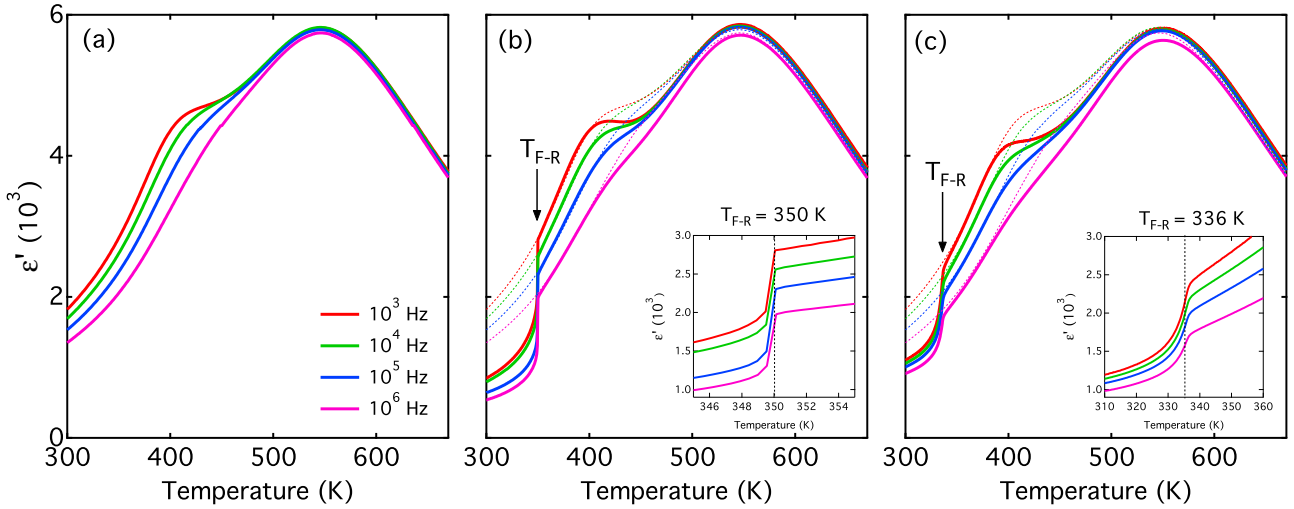

FIG. 1. Temperature-dependent relative permittivity of an unpoled (a), electrically poled (b), and mechanically textured (c) polycrystalline NBT-0.06BT sample. The mechanically poled sample was loaded to −500 MPa at 423 K for 5 min, whereas to the electrically poled sample a 2 kV/mm electric field was applied for 5 min at the same temperature. Both samples were subsequently field cooled to room temperature prior to testing. The dotted lines in (b,c) are the data for the unpoled sample.

Analogous mechanical field cooling–zero-field heating experiments were performed on mechanically textured NBT-0.06BT samples between room temperature and 423 K. Interestingly, the mechanically poled sample shows an almost identical temperature-dependent dielectric anomaly to the electrical case. This clearly demonstrates that an external uniaxial mechanical stress can also increase the correlation length of PNRs and induce a long-range ferroelectric order in relaxor ferroelectrics. Previous XRD measurements by Garg *et al.* on mechanically crushed NBT-xBT samples suggested a similarity between an electric-field-induced and a stress-induced phase transition [18]. However, the observed mechanical $T_{F\text{-}R}$ was found to be 336 K, approximately 14 K below the electrically poled sample. Please note that the measurement of the electrically poled sample was performed at a heating rate of 0.5 K/min instead of a rate of 2 K/min in the case of the mechanically textured sample. This could have an influence on the measured $T_{F\text{-}R}$, but a higher heating rate would increase the difference between the mechanically textured and the electrically poled sample. It could be expected that a higher $T_{F\text{-}R}$ would be observed for the electrically poled sample with increasing heating rates. Therefore the overall conclusions of the measurements presented here would not be affected. In addition, there is an apparent decrease in the temperature at which the frequency dispersive shoulder appears.

In this study, the transition temperature $T_{F\text{-}R}$ has also been shown to correspond to the depolarization temperature T_{dp}. This can be seen in temperature-dependent piezoelectric measurements (Fig. 2), where the piezoelectric response shows a sharp drop at $T_{F\text{-}R}$, corresponding to a loss of electrically induced domain structure due to a reverse transition from the long-range ferroelectric order to an ergodic relaxor state. These results are in contrast to observations made by Jo *et al.* in previous investigations, where a difference of several K was observed between T_{dp} and $T_{F\text{-}R}$ [21,23]. A possible reason for this discrepancy could be that the measurements in Fig. 2 were done at a heating rate of 0.5 K/min, whereas Jo *et al.* used 2 K/min. The lower heating rate probably led to a more quasistatic condition and therefore the two-stage process found by Jo *et al.* could not be observed. Another difference to the work of Jo *et al.* is that in the present study, both d_{33} and ε' were measured simultaneously in the same setup on the same sample, removing the possible difference in temperature measurements between different experimental arrangements.

Another interesting result of the measurement presented in Fig. 2 is the nonzero piezoelectric coefficient above the depolarization temperature. The value of d_{33} gradually decreases to zero with increasing temperature up to approximately 433 K, which could be roughly identified with the temperature at which the frequency dispersive shoulder in the permittivity-temperature curve ends. It is possible that remanent macroscopic polarization remains above T_{dp} in the temperature interval between $T_{F\text{-}R}$ and the end of the shoulder, which has previously been observed in measurements of the polarization as a function of temperature [21,23]. In addition, previous investigations by Jo *et al.* proposed that PNRs of both rhombohedral and tetragonal symmetries are present in NBT-0.06BT, where the rhombohedral PNRs gradually transform into tetragonal PNRs above $T_{F\text{-}R}$ [29]. PNRs with rhombohedral symmetry may still possess remanent macroscopic polarization, leading to a nonzero d_{33}.

In order to demonstrate the influence of holding time during texturizing, the same experiment shown in Fig. 1(c) was repeated and the mechanical compression was now applied for 1 h at −500 MPa instead of 5 min. This resulted in an increase in $T_{F\text{-}R}$ of 5−341 K, which can be likely attributed to a more complete texturing process from a longer holding time. In comparison, the magnitude of the applied compressive stress can also influence the completeness of the transition. Additional field cooling–zero-field heating dielectric measurements were performed on samples field cooled with a different constant bias compressive stress applied for 1 h at 423 K, shown in Fig. 3(a). For clarity, only the 1 kHz

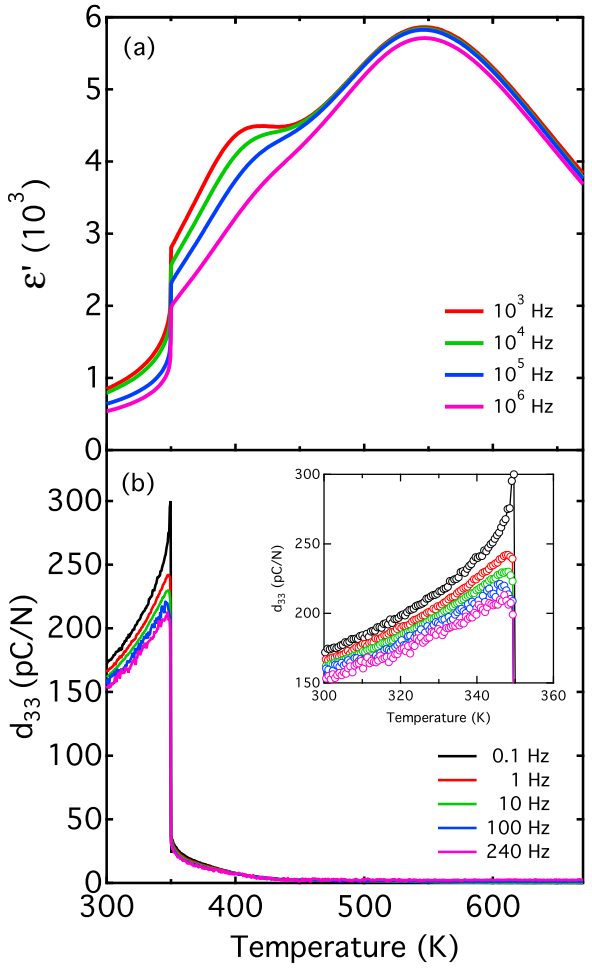

FIG. 2. Comparison of temperature-dependent relative permittivity ε' (a) and direct piezoelectric coefficient d_{33} (b) of electrically poled NBT-0.06BT.

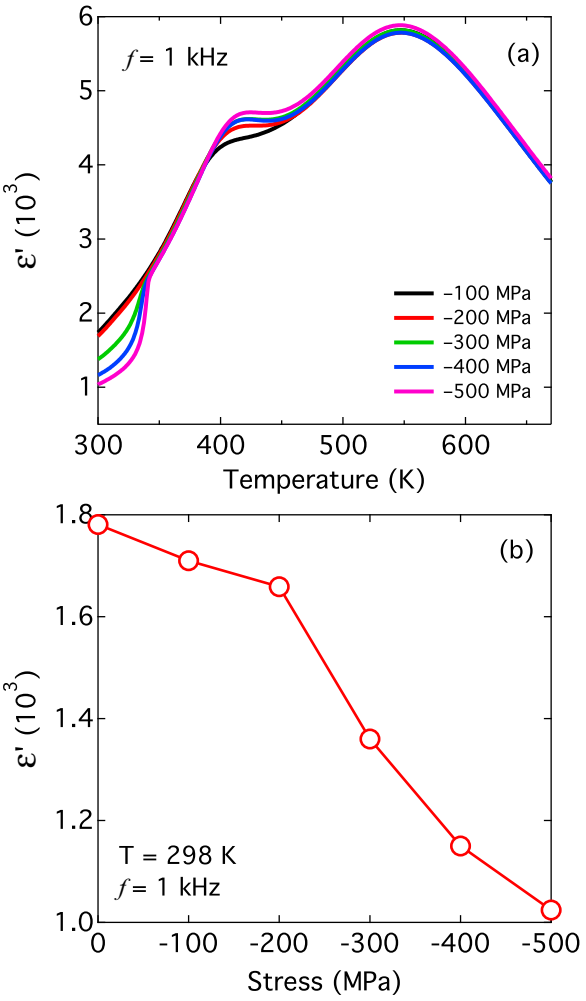

FIG. 3. Zero-field heating relative permittivity-temperature behavior for mechanically poled NBT-0.06BT samples measured at 1 kHz (a), and relative permittivity at 298 K as a function of bias stress (b). To each sample a different maximum compressive stress level was applied at 423 K for 1 h, prior to mechanical field cooling to room temperature.

dielectric data are presented. It is apparent from Fig. 3(a) that an increase in the bias stress increases the sharpness of the dielectric anomaly at $T_{F\text{-}R}$ during zero-field heating measurements as well as the higher-temperature shoulder. The relative permittivity at 298 K for each compressive texturing stress shows a continuous decrease [Fig. 3(b)]. Previous investigations on polycrystalline $Pb(Mg_{1/3}Nb_{2/3})O_3$-$PbTiO_3$ show a similar increase in the $T_{F\text{-}R}$ anomaly during field cooling–zero-field heating experiments with increasing poling electric field [59]. This was rationalized as an incomplete relaxor-to-ferroelectric transition at lower-electric-field levels, resulting in a mixed relaxor/ferroelectric state. An analog effect is expected in the mechanical case as well.

At compressive stresses up to approximately −200 MPa, for example, there is no clear development of a dielectric anomaly at $T_{F\text{-}R}$, although the room temperature relative permittivity was found to decrease by approximately 4% and 7% at −100 and −200 MPa, respectively, for the unpoled sample. At −300 MPa, however, there is the formation of an apparent dielectric anomaly, corresponding to a decrease in the room temperature relative permittivity of ∼24% compared to the unpoled sample. Interestingly, previous investigations found that the coercive stress of NBT-0.06BT at room temperature was approximately −275 MPa, corresponding well to the present experimental data [60]. There is, however, no clear saturation in the room temperature relative permittivity decrease, as would be expected when the relaxor-to-long-range ferroelectric order transition is exhausted.

Above the transition temperature, the dielectric response of each sample displays the same values until approximately 398 K, where a shoulder is observed. Here, there is again an apparent influence of mechanical loading, namely, with increasing mechanical texturing stress, the shoulder becomes more prominent. The origins of this effect are presently unclear, although it is interesting to note that the electrically poled samples display a similar prominent shoulder in the dielectric response in this region. Above approximately 473 K, each sample, regardless of applied mechanical texturing stress, displays the same high-temperature dielectric response up to 673 K.

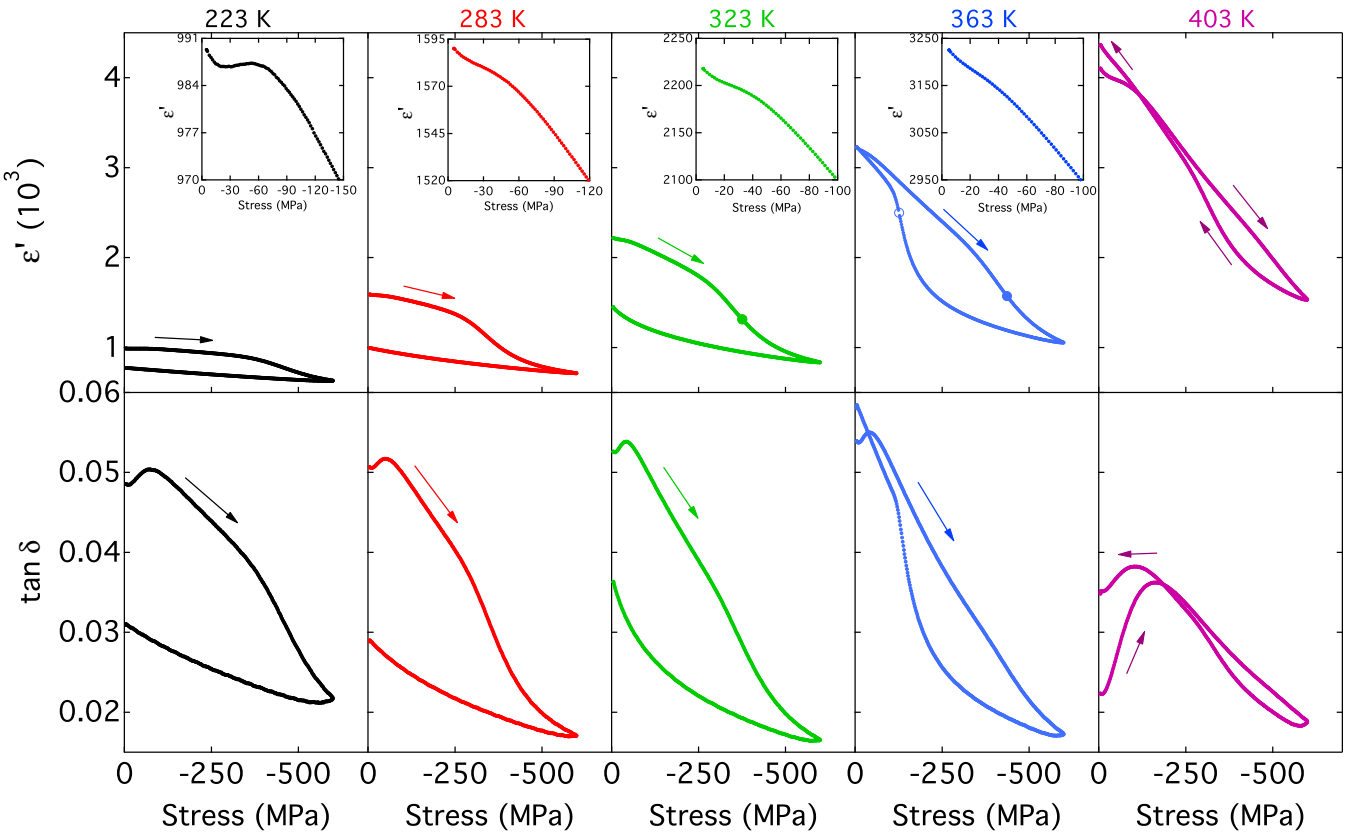

FIG. 4. Stress-dependent permittivity and loss tangent at various constant temperatures for polycrystalline NBT-0.06BT. To illustrate the critical forward RE-FE transition stress, determined by the inflection point in the relative permittivity curve during loading, a solid circle is shown for measurements performed at 323 and 363 K. The critical converse FE-RE transition stress, determined as the inflection point during unloading, is represented by an open circle, shown for data at 363 K. At 323 K, a converse FE-RE was not observed.

B. Dielectric response as a function of bias stress at constant temperature

To investigate the stress-induced RE-FE transition, the dielectric response of NBT-0.06BT was characterized during mechanical compressive loading up to −600 MPa at various constant temperatures between 223 and 433 K. Representative relative permittivity and dielectric loss data as a function of stress at five selected temperatures are shown in Fig. 4. At 223 K there is an approximately linear decrease in relative permittivity up to stresses of approximately −300 MPa, where a significant nonlinear change in the permittivity is observed. The origins of this decrease are probably the increased resistance to the motion of PNRs due to the uniaxial compression and the increasing correlation between the PNRs, resulting in a decreased response to the small electric field (1 V_{rms} at maximum) applied by the LCR meter.

At compressive stresses above the initial quasilinear portion, the NBT-0.06BT samples showed a nonlinear decrease in the relative permittivity and loss tangent resulting from the stress-induced RE-FE transition. The RE-FE transition stress was defined as the inflection point in the permittivity-stress curve during loading. At low temperatures, where the material is in the nonergodic state, this decrease was found to be remanent during unloading. With increasing temperature, there was an increase in the initial relative permittivity and a corresponding increase in the magnitude of the change observed during mechanical loading. This is due to the increased thermal fluctuations causing the material to be closer to the ergodic relaxor state. At 323 K it can be observed that there is an increased nonlinearity during unloading, which is the beginning of a converse FE-RE transition. At higher temperatures the FE-RE transition is complete and the relative permittivity-stress behavior forms a closed loop. The closed loop behavior observed here, however, does not correspond to the macroscopic mechanical constitutive behavior previously observed by Webber *et al.* for unpoled, virgin NBT-0.06BT [60], where the stress-strain behavior at 373 K displayed a remanent strain characteristic of typical ferroelasticity. In addition, the coercive stress of NBT-0.06BT was found to be approximately −200 MPa at 363 K, which does not clearly correspond to any of the features in the relative permittivity– or loss tangent–stress curve presented here. This indicates an apparent decoupling between the macroscopic stress-strain response and the stress-induced RE-FE transition behavior.

Upon closer examination of the low-stress region (up to −150 MPa) a nonlinear effect represented by a maximum in the relative permittivity at −51 MPa at 223 K is revealed (shown in the insets in Fig. 4). This effect is more clearly seen in the dielectric loss data. The origins of this low-stress

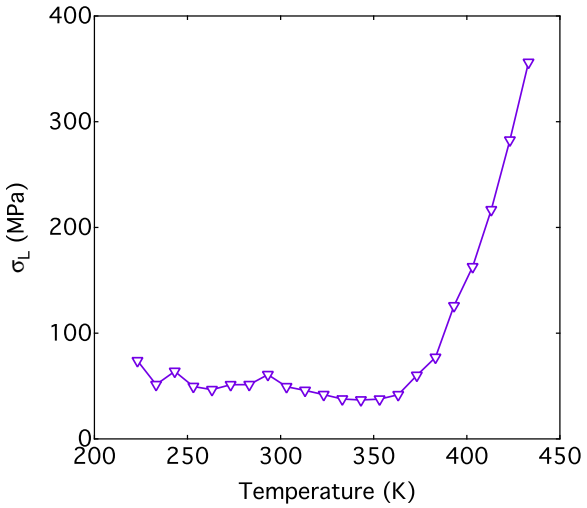

FIG. 5. Stress at peak loss tangent as a function of temperature during load increase.

nonlinearity are presently unclear, but could potentially be due to reorientation or clamping of PNRs at mechanical loads below the critical RE-FE transition stress. In mixed phase systems, such as NBT-xBT near the MPB, it is also possible that nanopolar regions of differing symmetry respond differently to the applied mechanical load and that the texturing response of one phase might be responsible for the loss tangent peak. Indeed, Ma *et al.* [8] reported the transition of $P4bm$ nanodomains into thin lamellar domain structures during the application of a dc electric field in NBT-0.06BT. This transition occurred below the coercive field and was not accompanied by a structural phase transition [61]. A similar effect during mechanical loading is also possible, resulting in the observed dielectric response at lower stresses. A previous investigation by Bobnar *et al.* also revealed an analogous dielectric nonlinearity in $Pb_{1-x}La_x(Zr_yTi_{1-y})_{1-x/4}O_3$ during electric-field loading at constant temperature, although no possible mechanism was suggested [28]. At 223 K the dielectric loss peak occurs at a stress of −70 MPa, which does not coincide with the initial maximum in permittivity described above. With increasing temperature up to 363 K there is an apparent decrease in this stress to approximately −42 MPa. At 403 K, the peak again becomes more prominent and occurs at an applied stress of −160 MPa. Figure 5 shows the stress at maximum dielectric loss σ_L as a function of temperature. Above 350 K there is a sharp increase in σ_L, perhaps suggesting a decreased influence of external mechanical fields on the clamping or reorientation of PNRs. This corresponds to the observed increase in the critical RE-FE transition stress and the transition to the ergodic relaxor state (Fig. 4).

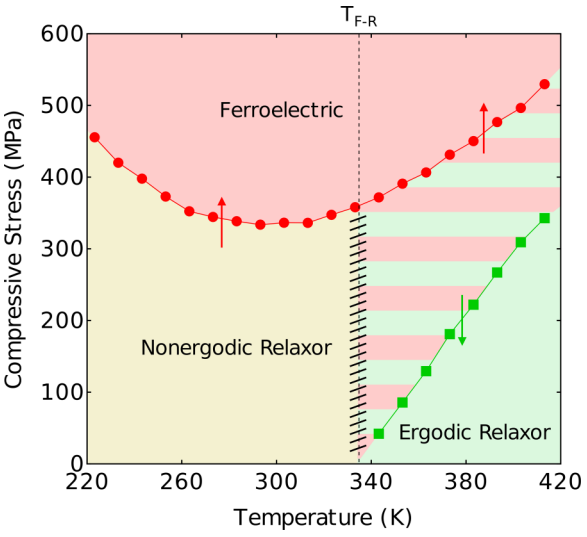

FIG. 6. Stress-temperature phase diagram for NBT-0.06BT. $T_{F\text{-}R}$ for mechanically textured sample determined by temperature-dependent relative permittivity measurements is marked by a dashed line. The arrows represent the loading direction, whereas the red/green hatched region symbolizes that the phase depends on the loading direction in this region, i.e., ergodic during loading and ferroelectric during unloading.

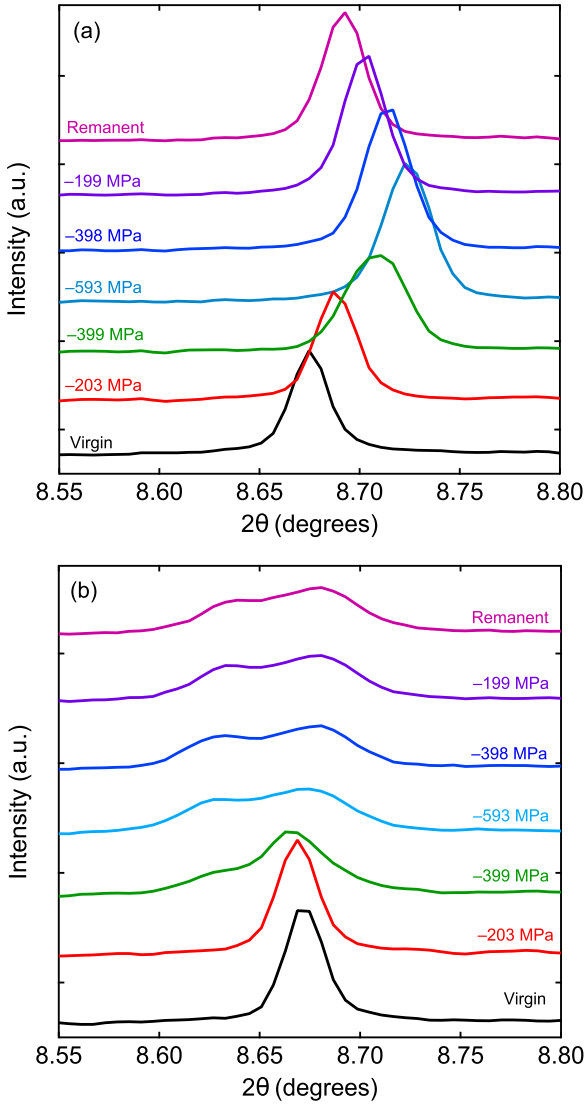

FIG. 7. Stress dependence of the 222_{PC} peaks parallel (a) and perpendicular (b) to the applied compressive stress.

C. Stress-temperature phase diagram

From the stress-dependent relative permittivity measurements at constant temperature (Fig. 4), the critical stresses during loading and unloading, corresponding to the RE-FE and FE-RE transitions, respectively, were determined. These critical stresses are shown in the stress-temperature phase diagram (Fig. 6), where the ferroelectric, nonergodic relaxor and ergodic relaxor regions are highlighted. As previously mentioned, the inflection point in the relative permittivity-stress curve was taken as the transition point. It is important to note, however, that the proposed phase boundaries are continuous in nature, as can be seen in Fig. 3, where an increase in compressive texturing stress leads to a progressive increase in ferroelectric long-range order, and should only be read in the stress direction. An extrapolation of the converse RE-FE transition line in Fig. 6 to zero stress reveals a transition temperature of 335 K. At temperatures below 335 K without applied compressive stress, NBT-0.06BT is in a nonergodic relaxor state. This temperature also corresponds well to the observed $T_{F\text{-}R}$ of the mechanically textured sample (Fig. 1). During mechanical loading the stress-induced RE-FE transition is metastable, i.e., a converse FE-RE transition upon unloading is not observed. In this region, polarization– and strain–electric-field hysteresis loops, typical of a normal ferroelectric, are observed after the first half cycle [21]. At temperatures above 335 K, NBT-0.06BT is an ergodic relaxor, which results in a reversible FE-RE transition upon mechanical unloading due to increased thermal fluctuations acting to break down the stress-induced long-range order. The direction of the RE-FE and FE-RE transitions are denoted by arrows in Fig. 6. The stress-temperature phase diagram has the same form as previous electric-field–temperature phase diagrams presented for Mn-doped NBT-0.06BT [48] further indicating the parallels of electrical and mechanically modulated RE-FE transitions in relaxor ferroelectrics.

D. Stress-dependent synchrotron diffraction

To determine the crystallography of the stress-induced RE-FE phase transition, *in situ* high-energy synchrotron x-ray diffraction measurements were performed on polycrystalline NBT-0.06BT, mechanically loaded in compression at room temperature. Figure 7 shows the stress-dependent diffraction patterns near the 222_{PC} reflection recorded with the scattering vectors parallel and perpendicular to the applied stress. Here, the subscript PC is used to denote the peak types in the parent cubic perovskite unit cell. The 222_{PC} reflections with the scattering vector aligned parallel to the applied stress [Fig. 7(a)] remain single and symmetric, however, significant stress-induced peak broadening and lattice strain were observed as peak shifts. The development of a remanent lattice strain was also detected from these data after the removal of the applied stress. In contrast, patterns with the scattering vector perpendicular to the applied stress [Fig. 7(b)] show the 222_{PC} peaks split into multiple reflections at high stresses larger than −203 MPa. These observations are consistent with a stress-induced phase transition from the initial pseudocubic

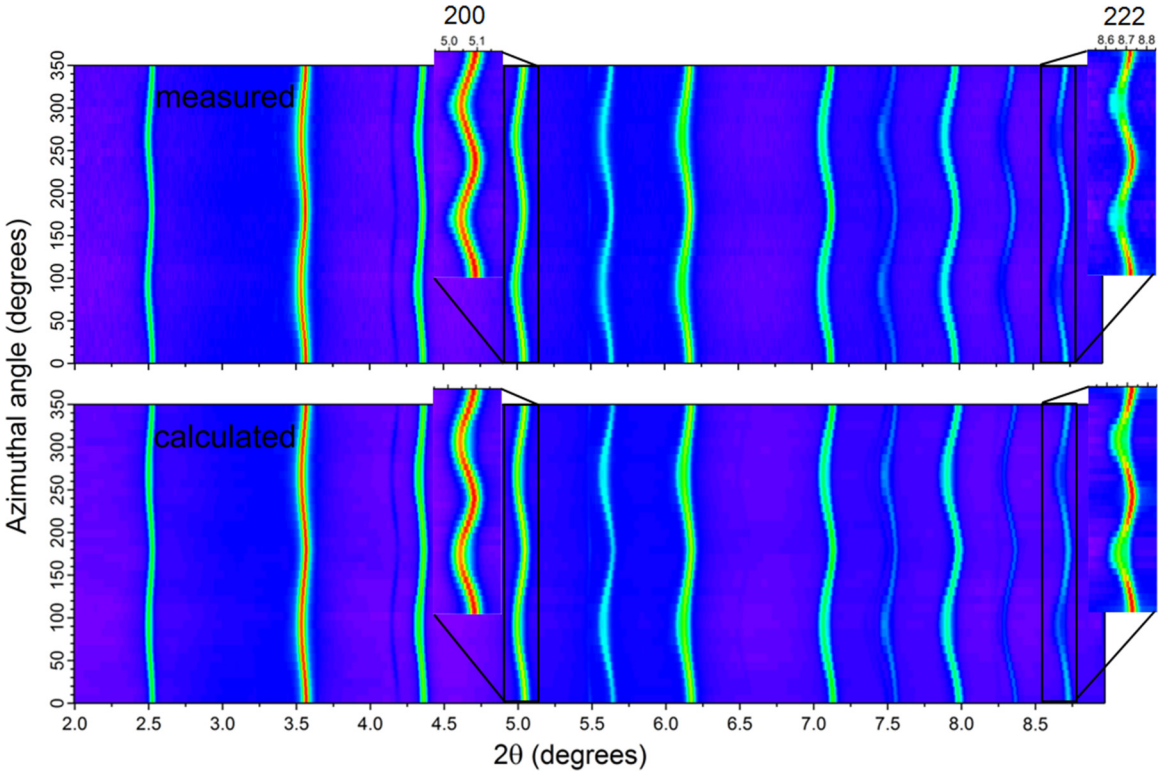

FIG. 8. Contour plots of the measured and calculated XRD patterns using the $R3c + P4mm$ structural model at −593 MPa and as a function of the angle of the scattering vector with respect to the applied compressive stress (azimuthal angle). The insets show the characteristic 200_{PC} and 222_{PC} reflections.

phase to a possible mixed rhombohedral-tetragonal phase structure with a non-180° ferroelectric domain texture. The rhombohedral distortion preferentially takes place in the grains oriented with a $\langle 111\rangle_{PC}$ axis perpendicular to the applied stress; thus the domain texture is most obvious when measuring in this orientation. The diffraction measurement of the sample after mechanical loading reveals that the stress-induced phase transition is irreversible, analogous in nature to the electric-field-induced phase transition observed in the unpoled NBT-xBT material [8,19,21,62].

In order to quantify the full crystallographic nature of the transition, Rietveld refinements incorporating texture models were performed as a function of the applied stress over the whole mechanical loading/unloading process. Firstly, three different structural models including $R3c$, $R3c + P4mm$, and $R3c + Pm\bar{3}m$ were considered at the maximum stress state. Based on the fit quality parameter, R_{wp}, which describes the weighed discrepancy between the measured and calculated intensities, the $R3c + P4mm$ model gives the best quality fit. In addition, a close comparison of the measured and calculated patterns indicates that the $R3c + P4mm$ model comprehensively reproduces subtle features of the diffraction patterns at high stresses (as shown in Fig. 8), which are not reproduced by the other two models.

This model was then applied sequentially to the entire diffraction data set measured during mechanical loading. In each instance, the lattice and texture parameters were refined. Figure 9 shows the lattice distortions and phase fractions of $R3c$ and $P4mm$ phases as a function of the applied stress. It was found that when the structures are refined as $R3c$ and $P4mm$ for stresses below −203 MPa, the two phases both appear to have approximately zero distortion (η) from the parent pseudocubic state ($\eta_T < 0.05\%$, $\eta_R < 0.04\%$); thus the material is considered pseudocubic before −203 MPa. Similar observations were made during electrical loading of NBT-0.06BT [29]. Moreover, we confirm the fits are reasonable using a single-phase cubic model $Pm\bar{3}m$ at stresses up to −203 MPa. Note that in the structural analysis we assume that the initial pseudocubic $Pm\bar{3}m$ phase completely transforms to $R3c + P4mm$ phases when the applied stress is above a critical value of around −203 MPa. With the current diffraction data, it is difficult to discern a stress region (above −203 MPa) with the coexistence of $Pm\bar{3}m + R3c + P4mm$ phases, despite this being likely when considering the permittivity measurements presented above.

Between stresses of approximately −203 and −400 MPa during the loading cycle, an increasing lattice distortion in the initially dominant $R3c$ phase was observed [Fig. 9(a)] to coincide with the development of the tetragonal $P4mm$ phase fraction [Fig. 9(b)]. The quantitative phase analysis also indicates that during compressive loading (above −203 MPa), the stress-induced interferroelectric phase transition from $R3c$ to $P4mm$ occurs [63], and this phase transition is irreversible during unloading. The refinement result in Fig. 9(a) also highlights that the lattice distortions of the $R3c$ and $P4mm$ phases, in response to the compressive stress, are significantly different. As summarized in Table I, the rhombohedral $R3c$ phase shows an active response to the applied stress, achieving a significant lattice distortion $\eta_R = 0.8447\%$ with 49.6%

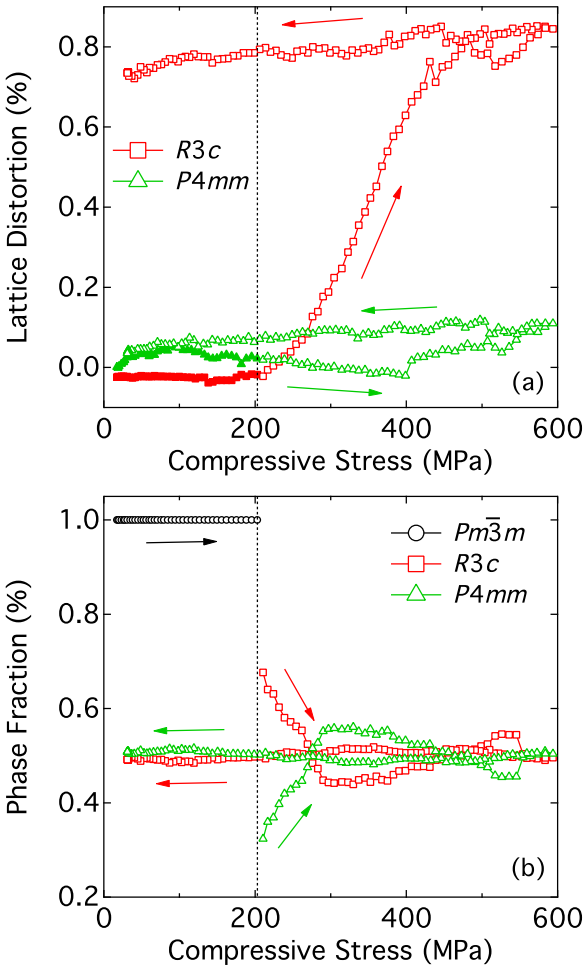

FIG. 9. (a) The lattice distortion of $R3c$ and $P4mm$ phases and (b) the phase fractions as a function of compressive stress. For the $R3c$ phase, the lattice distortion $\eta_R = c_H/\sqrt{6}a_H - 1$ (a_H and c_H are the unit cell parameters represented in hexagonal axes); for the $P4mm$ phase, $\eta_T = c_T/a_T - 1$. The filled symbols in (a) denote the lattice distortions of $R3c$ and $P4mm$ phases below the critical stress (−203 MPa), depicted with a dotted line. The arrows show the loading direction.

TABLE I. Refined structural parameters of mechanically poled NBT-0.06BT (−593 MPa) with the $R3c + P4mm$ model. η is the lattice distortion, for the tetragonal $P4mm$ phase $\eta_T = c_T/a_T - 1$, and for the rhombohedral $R3c$ phase $\eta_R = c_H/\sqrt{6}a_H - 1$. R_{wp} and R_p represent the quality of fit obtained by the structural model.

Structures (−593 MPa)	$P4mm$	$R3c$ (represented in hexagonal axes)
a (Å)	3.89919(4)	5.49954(8)
c (Å)	3.90349(10)	13.58487(43)
η (%)	0.1102(15)	0.8447(17)
Phase fraction (%)	50.4(8)	49.6(6)
R_{wp} (%)	8.788	
R_p (%)	5.453	

rhombohedral phase at a maximum stress of −593 MPa. In contrast, the $P4mm$ phase exhibits a very small tetragonal distortion under stress with only $\eta_T = 0.11\%$ developed within the 50.4% tetragonal phase at −593 MPa.

From Fig. 9, it is apparent that during compressive mechanical loading NBT-0.06BT undergoes a structural transformation, analogous to previous observations during electrical loading of $(1-x-y)(Bi_{0.5}Na_{0.5})TiO_3$-$xBaTiO_3$-$y(K_{0.5}Na_{0.5})NbO_3$ [27,64]. This is understood to be due to transition from a relaxor state to long-range ferroelectric order, consistent with the increase in PNR correlation length [8,49]. The unit cell volume for each phase was determined as a function of compressive stress. A decrease in the unit cell volume of approximately −0.07% between the initial and remanent states was observed, which indicates a ferroelastic reorientation of PNRs into long-range order as well as a field-induced interferroelastic transition. This is consistent with diffraction data that show changing $R3c$ and $P4mm$ volume fractions during mechanical loading. The completeness of the RE-FE transition was found to depend on the thermal and mechanical history of the sample, where samples textured at high temperature (423 K) displayed an increased dielectric anomaly at $T_{F\text{-}R}$ with increasing texturing stress (Fig. 3). Stresses up to −200 MPa did not significantly change the room temperature relative permittivity. This corresponds well to XRD results, which show the onset of a $Pm\bar{3}m$ to mixed $R3c + P4mm$ transition at approximately −203 MPa. Above this critical stress there is an apparent structural phase transition accompanied by a development and subsequent increase of lattice distortion of the $R3c$ and $P4mm$ phases with increasing stress. In comparison with Fig. 6 this load could be considered as the onset stress for the induced phase transition, whereas the values in Fig. 6 are defined via the inflection point of the permittivity curve as a function of load. The inflection points represent the stresses where the rate of the phase transition process was at maximum, indicating that the phase transition did not take place at a specific stress but rather over a stress range. There was no clear explanation of the low-stress dielectric and loss tangent anomaly from the diffraction data.

IV. SUMMARY

The lead-free relaxor material NBT-0.06BT was found to undergo a stress-induced transition from the relaxor state to a state of long-range ferroelectric order. Mechanical texturing resulted in the formation of a dielectric anomaly at $T_{F\text{-}R}$ during field cooling–zero-field heating experiments, consistent with earlier reports on the effect of electrical poling of other relaxor ferroelectrics, such as $Pb(Mg_{1/3}Nb_{2/3})O_3$, $Pb_{1-x}La_x(Zr_yTi_{1-y})_{1-x/4}O_3$ and $(1\text{-}x)Pb(Mg_{1/3}Nb_{2/3})O_3$-$xPbTiO_3$. The relative permittivity and dielectric loss were characterized as a function of compressive stress on virgin samples at various constant temperatures between 223 and 413 K. These measurements revealed a metastable RE-FE transition at temperatures below 335 K, where NBT-0.06BT is understood to be in a nonergodic relaxor state. Above 335 K, NBT-0.06BT is an ergodic relaxor, resulting in a converse FE-RE transition during mechanical unloading due to the increased thermal fluctuations. A stress-temperature phase diagram for NBT-0.06BT was proposed. *In situ* high-energy synchrotron x-ray diffraction measurements were performed to investigate the effect of applied stress on the crystal structure. A structural transition from $Pm\bar{3}m$ to mixed $R3c + P4mm$ was observed, corresponding well with the macroscopic property measurements.

ACKNOWLEDGMENTS

F.H.S. and K.G.W. gratefully acknowledge financial support from the Deutsche Forschungsgemeinschaft under Grant No. WE 4972/2-1. We acknowledge the European Synchrotron Radiation Facility for the provision of experimental beam time for carrying out the *in situ* diffraction measurements. This work was supported in part through Australian Research Council Projects No. DP120103968, No. DP130100415, and No. DE150100750 as well as the Bundesministerium für Bildung und Forschung Project No. 05K13VK1.

[1] T. Takenaka, K.-I. Maruyama, and K. Sakata, Jpn. J. Appl. Phys. **30**, 2236 (1991).
[2] P. K. Panda, J. Mater. Sci. **44**, 5049 (2009).
[3] V. V. Shvartsman, D. C. Lupascu, and D. J. Green, J. Am. Ceram. Soc. **95**, 1 (2012).
[4] J. Rödel, K. G. Webber, R. Dittmer, W. Jo, M. Kimura, and D. Damjanovic, J. Eur. Ceram. Soc. **35**, 1659 (2015).
[5] G. O. Jones and P. A. Thomas, Acta Crystallogr., Sect. B: Struct. Sci. **58**, 168 (2002).
[6] G. Picht, J. Töpfer, and E. Hennig, J. Eur. Ceram. Soc. **30**, 3445 (2010).
[7] W. Jo, J. E. Daniels, J. L. Jones, X. Tan, P. A. Thomas, D. Damjanovic, and J. Rödel, J. Appl. Phys. **109**, 014110 (2011).
[8] C. Ma, H. Guo, S. P. Beckman, and X. Tan, Phys. Rev. Lett. **109**, 107602 (2012).
[9] S.-T. Zhang, A. B. Kounga, E. Aulbach, T. Granzow, W. Jo, H.-J. Kleebe, and J. Roödel, J. Appl. Phys. **103**, 034107 (2008).
[10] M. Chen, Q. Xu, B. H. Kim, B. K. Ahn, J. H. Ko, W. J. Kang, and O. J. Nam, J. Eur. Ceram. Soc. **28**, 843 (2008).
[11] C. Xu, D. Lin, and K. W. Kwok, Solid State Sci. **10**, 934 (2008).
[12] S.-T. Zhang, A. B. Kounga, E. Aulbach, and Y. Deng, J. Am. Ceram. Soc. **91**, 3950 (2008).
[13] H. Simons, J. E. Daniels, J. Glaum, A. J. Studer, J. L. Jones, and M. Hoffman, Appl. Phys. Lett. **102**, 062902 (2013).
[14] J. Kling, X. Tan, W. Jo, H. J. Kleebe, H. Fuess, and J. Rödel, J. Am. Ceram. Soc. **93**, 2452 (2010).
[15] C. Ma and X. Tan, Solid State Commun. **150**, 1497 (2010).
[16] L. A. Schmitt, J. Kling, M. Hinterstein, M. Hoelzel, W. Jo, H. J. Kleebe, and H. Fuess, J. Mater. Sci. **46**, 4368 (2011).
[17] R. Ranjan and A. Dviwedi, Solid State Commun. **135**, 394 (2005).
[18] R. Garg, B. N. Rao, A. Senyshyn, P. S. R. Krishna, and R. Ranjan, Phys. Rev. B **88**, 014103 (2013).

[19] J. E. Daniels, W. Jo, J. Rödel, and J. L. Jones, Appl. Phys. Lett. **95**, 032904 (2009).
[20] H. Foronda, M. Deluca, E. Aksel, J. S. Forrester, and J. L. Jones, Mater. Lett. **115**, 132 (2014).
[21] W. Jo, R. Dittmer, M. Acosta, J. Zang, C. Groh, E. Sapper, K. Wang, and J. Rödel, J. Electroceram. **29**, 71 (2012).
[22] E. Sapper, S. Schaab, W. Jo, T. Granzow, and J. Roödel, J. Appl. Phys. **111**, 014105 (2012).
[23] W. Jo, J. Daniels, D. Damjanovic, W. Kleemann, and J. Roödel, Appl. Phys. Lett. **102**, 192903 (2013).
[24] D. I. Woodward, R. Dittmer, W. Jo, D. Walker, D. S. Keeble, M. W. Dale, J. Rödel, and P. A. Thomas, J. Appl. Phys. **115**, 114109 (2014).
[25] F. Cordero, F. Craciun, F. Trequattrini, E. Mercadelli, and C. Galassi, Phys. Rev. B **81**, 144124 (2010).
[26] R. Dittmer, W. Jo, K. G. Webber, J. L. Jones, and J. Rödel, J. Appl. Phys. **115**, 084108 (2014).
[27] J. E. Daniels, W. Jo, J. Rödel, V. Honkimäki, and J. L. Jones, Acta Mater. **58**, 2103 (2010).
[28] V. Bobnar, Z. Kutnjak, R. Pirc, and A. Levstik, Phys. Rev. B **60**, 6420 (1999).
[29] W. Jo, S. Schaab, E. Sapper, L. A. Schmitt, H. J. Kleebe, A. J. Bell, and J. Rödel, J. Appl. Phys. **110**, 074106 (2011).
[30] I. P. Raevski, S. A. Prosandeev, A. S. Emelyanov, S. I. Raevskaya, E. V. Colla, D. Viehland, W. Kleemann, S. B. Vakhrushev, J.-L. Dellis, M. El Marssi, and L. Jastrabik, Phys. Rev. B **72**, 184104 (2005).
[31] Z. Kutnjak, B. Vodopivec, and R. Blinc, Phys. Rev. B **77**, 054102 (2008).
[32] J. Hlinka, J. Adv. Dielect. **02**, 1241006 (2012).
[33] G. Burns and F. H. Dacol, Solid State Commun. **48**, 853 (1983).
[34] P. Bonneau, P. Garnier, G. Calvarin, E. Husson, J. R. Gavarri, A. W. Hewat, and A. Morell, J. Solid State Chem. **91**, 350 (1991).
[35] G. Burns and F. H. Dacol, Phys. Rev. B **28**, 2527 (1983).
[36] C. Boulesteix, F. Varnier, A. Llebaria, and E. Husson, J. Solid State Chem. **108**, 141 (1994).
[37] M. A. Akbas and P. K. Davies, J. Am. Ceram. Soc. **80**, 2933 (1997).
[38] L. E. Cross, Ferroelectrics **76**, 241 (1987).
[39] D. Viehland, S. J. Jang, L. E. Cross, and M. Wuttig, J. Appl. Phys. **68**, 2916 (1990).
[40] Y. Imry and S.-k. Ma, Phys. Rev. Lett. **35**, 1399 (1975).
[41] V. V. Westphal, W. Kleemann, and M. D. Glinchuk, Phys. Rev. Lett. **68**, 847 (1992).
[42] A. E. Glazounov and A. K. Tagantsev, Ferroelectrics **221**, 57 (1999).
[43] R. Pirc and R. Blinc, Phys. Rev. B **60**, 13470 (1999).
[44] A. A. Bokov and Z.-G. Ye, J. Mater. Sci. **41**, 31 (2006).
[45] R. Sommer, N. K. Yushin, and J. J. van der Klink, Phys. Rev. B **48**, 13230 (1993).
[46] Z.-G. Ye and H. Schmid, Ferroelectrics **145**, 83 (1993).
[47] M. Davis, D. Damjanovic, and N. Setter, Phys. Rev. B **73**, 014115 (2006).
[48] E. Sapper, N. Novak, W. Jo, T. Granzow, and J. Rödel, J. Appl. Phys. **115**, 194104 (2014).
[49] G. A. Samara, J. Phys.: Condens. Matter **15**, R367 (2003).
[50] M. Hinterstein, M. Hoelzel, J. Rouquette, J. Haines, J. Glaum, H. Kungl, and M. Hoffman, Acta Mater. **94**, 319 (2015).
[51] F. H. Schader, M. Morozov, E. T. Wefring, T. Grande, and K. G. Webber, J. Appl. Phys. **117**, 194101 (2015).
[52] J. E. Daniels and M. Drakopoulos, J. Synchrotron Radiat. **16**, 463 (2009).
[53] A. P. Hammersley, S. O. Svensson, M. Hanfland, A. N. Fitch, and D. Hausermann, High Press. Res. **14**, 235 (1996).
[54] S. Matthies, L. Lutteroti, and H. R. Wenk, J. Appl. Crystallogr. **30**, 31 (1997).
[55] N. C. Popa and D. Balzar, J. Appl. Crystallogr. **47**, 2113 (2014).
[56] B. Wylie-van Eerd, D. Damjanovic, N. Klein, N. Setter, and J. Trodahl, Phys. Rev. B **82**, 104112 (2010).
[57] O. Bidault, M. Licheron, E. Husson, and A. Morell, J. Phys.: Condens. Matter **8**, 8017 (1996).
[58] E.-M. Anton, W. Jo, D. Damjanovic, and J. Roödel, J. Appl. Phys. **110**, 094108 (2011).
[59] J. Peräntie, J. Hagberg, A. Uusimäki, and H. Jantunen, Appl. Phys. Lett. **93**, 132905 (2008).
[60] K. G. Webber, Y. Zhang, W. Jo, J. E. Daniels, and J. Rödel, J. Appl. Phys. **108**, 014101 (2010).
[61] H. Guo, C. Ma, X. Liu, and X. Tan, Appl. Phys. Lett. **102**, 092902 (2013).
[62] H. Simons, J. Daniels, W. Jo, R. Dittmer, A. Studer, M. Avdeev, J. Rödel, and M. Hoffman, Appl. Phys. Lett. **98**, 082901 (2011).
[63] H. Fu and R. E. Cohen, Nature **403**, 281 (2000).
[64] M. Hinterstein, M. Knapp, M. Hölzel, W. Jo, A. Cervellino, H. Ehrenberg, and H. Fuess, J. Appl. Crystallogr. **43**, 1314 (2010).